Bioactive Materials 12 (2022) 133–142

Contents lists available at ScienceDirect

Bioactive Materials

journal homepage: www.keaipublishing.com/en/journals/bioactive-materials

Microfluidics-assisted optimization of highly adhesive haemostatic hydrogel coating for arterial puncture

Xingjie Yin [a,1], Jingli Ren [b,1], Wei Lan [c], Yu Chen [b], Mengping Ouyang [b], Hua Su [a], Lianbin Zhang [b], Jintao Zhu [b], Chun Zhang [a,*]

[a] Department of Nephrology, Union Hospital, Tongji Medical College, Huazhong University of Science and Technology Wuhan, 430022, China
[b] Key Lab of Material Chemistry for Energy Conversion and Storage of Ministry of Education, School of Chemistry and Chemical Engineering, Huazhong University of Science and Technology, Wuhan, 430074, China
[c] State Key Laboratory of Coal Combustion and School of Energy and Power Engineering, Huazhong University of Science and Technology, Wuhan, 430074, China

ARTICLE INFO

Keywords:
Gelatin hydrogel
Underwater adhesive
Microfluidics
Haemostatic coating
Vessel puncture

ABSTRACT

Although common in clinical practice, bleeding after tissue puncture may cause serious outcomes, especially in arterial puncture. Herein, gelatin-tannic acid composite hydrogels with varying compositions are prepared, and their adhesive properties are further optimized in microfluidic channel-based simulated vessels for haemostasis in arterial puncture. It is revealed that the composite hydrogels on the syringe needles used for arterial puncture should possess underwater adhesion higher than 4.9 kPa and mechanical strength higher than 86.0 kPa. The needles coated with the gelatin-tannic acid composite hydrogel completely prevent blood loss after both vein and arterial puncture in different animal models. This study holds great significance for the preparation of haemostatic needles for vessel puncture, and gelatin-tannic acid hydrogel coated needles may help to prevent complications associated with arterial puncture.

1. Introduction

Tissue puncture, including vessel puncture and viscera puncture, is a commonly used method for drug delivery and sampling in disease diagnosis and treatment [1–3]. Bleeding after tissue puncture is the main complication and not only causes psychological fear in patients but also increases the risk of infection and even hemorrhagic shock [4–6]. Manual compression and patient immobilization are usually used to achieve haemostasis after tissue puncture, which usually takes a few minutes to hours and is often associated with patient discomfort, subcutaneous ecchymosis, local hematoma, and even re-bleeding [7,8]. In addition, for patients whose coagulation function is abnormal (e.g., haemophilia), traditional haemostatic methods usually fail, and the tissue puncture turns out to be a contraindication due to haemorrhage [9,10]. Therefore, developing strategies for controlling haemorrhage after tissue puncture is highly desirable, and to this end, tremendous efforts have been dedicated to the progress of haemostatic methods for the rapid avoidance of blood loss after tissue puncture, such as the XStat™ device, injectable hydrogels, miniature sponges, and haemostatic needles [11–14].

Among the recently developed haemostatic strategies, *in situ* haemostasis by functionalized needles is attracting growing interest, as these needles can achieve synchronous, effective, and complete haemostasis after needle extraction, regardless of whether the patients have coagulation dysfunction, and can avoid postoperative complications [12,15]. Haemostatic needles are usually obtained by coating the needle surface with hydrogels, such as catechol/Lys-conjugated chitosan, chitosan-catechol-poly (*N*-isopropyl acrylamide), and alginate--$CaCl_2$-based hydrogels, which can undergo an *in situ* solid-to-hydrogel phase transition to physically seal puncture wounds and achieve haemostasis after tissue puncture [15–17]. Recently, Lee et al. reported haemostatic needles coated with partially crosslinked catechol-functionalized chitosan and showed immediate and complete haemostasis after vein puncture [12]. Although these coated needles effectively stop bleeding of vein puncture, achieving *in situ* haemostasis remains challenging in arterial puncture, which is widely employed to

Peer review under responsibility of KeAi Communications Co., Ltd.
* Corresponding author.
E-mail address: drzhangchun@hust.edu.cn (C. Zhang).
[1] These authors contributed equally to this work.

https://doi.org/10.1016/j.bioactmat.2021.10.009
Received 12 July 2021; Received in revised form 19 September 2021; Accepted 4 October 2021
Available online 11 October 2021

diagnose and treat diseases, such as arterial blood gas analysis, selective angiography and treatment, cardiac catheterization, and hemodialysis [18–20]. The high pressure and blood flow rate of the artery may remove or break up the adhesive hydrogels owing to their limited underwater adhesion and weak bonding mechanic [21]. On the other hand, the infeasibility of observation and detection *in vivo* hinders the optimization of adhesive hydrogels. Therefore, it is of great significance to explore methods for evaluating the underwater adhesive and mechanical properties of haemostatic hydrogels according to the hemodynamic characteristics of blood vessels and then to design and optimize haemostatic coatings to achieve haemostasis in arterial puncture.

Microfluidic technology is widely used to precisely control small volumes of fluid and its flow in microchannels. Microfluidic channels provide ideal platforms to simulate the flow conditions of different blood vessels in vitro and visually evaluate the performance of haemostatic hydrogels [22]. Aiming to develop haemostatic needles for arterial puncture, in the current study, we employed a microfluidic system to optimize the underwater adhesion of a rationally designed gelatin-tannic acid hydrogel coating. Tannic acid (TA), a naturally derived polyphenol compound, has exhibited valuable properties such as antibacterial and anti-inflammatory characteristics as well as good biocompatibility and biodegradability [23,24]. TA can form different adhesive strength hydrogel with neutral polymers and proteins (e.g., gelatin or collagen) *via* multiple reaction pathways, including through covalent bonding, hydrogen bonding, electrostatic interactions, and hydrophobic interactions [25–27]. Gelatin-TA hydrogel (Gel-TA) was prepared *via* covalent bonding reaction pathways between TA and gelatin [28]. By optimizing the proportion of TA, we synthesized Gel-TA with a TA mass content of 2%, which has high underwater adhesion, strong mechanical strength, and large bursting pressure. By manipulating and controlling the microfluidic platform and miniaturized devices with vessel-sized channels, we clarified the relationship between the adhesion properties of hydrogels and blood pressure and showed that the hydrogels used for arterial haemostasis should have a high underwater adhesion of 4.9 kPa and a tough mechanical strength of 86.0 kPa. Finally, we produced haemostatic needles by applying the Gel-TA to the surface of the syringe needles, and the results showed that, for both vein and arterial puncture in different animal models, the haemostatic needles exhibited synchronous haemostasis through a solid-to-gel phase transition. The current study opens up a way for designing and optimizing haemostatic needles, and the Gel-TA-coated haemostatic needles hold enormous potential for clinical arterial puncture.

2. Materials and methods

2.1. Materials

Ethanol was purchased from Sinopharm Co. Ltd. (Shanghai, China). Cyanine 5 amine (Cy5-NH_2) was obtained from Lumiprobe Corporation. Gelatin, TA, *N*-(3-dimethylaminopropyl)-*N′*-ethylcarbodiimide hydrochloride (EDC. HCl, 98%), and fluorescein isothiocyanate isomer (FITC) were supplied by Aladdin (Shanghai, China).

2.2. Preparation of gelatin-tannic acid solutions

Dissolve 100 mg of gelatin in 9.9 g of deionized water and then a gelatin solution (1 wt%) was prepared. TA (200 mg) was added to 9.8 g of deionized water. Mix the above two solution and stir to obtain homogeneous solution. The solution was adjusted to pH 8 and stored at room temperature for two days. Similarly, prepare Gel-TA solutions with varied TA contents (1 wt%, 2 wt%, 3 wt%, and 4 wt%) according to the above process.

2.3. Preparation of FITC-Gel-TA, RhB-alginate-$CaCl_2$ (RhB-Alg) hydrogel, and fluorescein-sodium-decorated fibrin glue

The FITC-Gel-TA, RhB-Alg and fluorescein-sodium-decorated fibrin glue were prepared as previously reported 1 [7,29]. The small simulation hydrogel used for microfluidics was prepared by blade cutting under a microscope.

2.4. Preparation of liposome-decorated silicone tubes

First, liposomes were prepared according to previous reports [30]. Typically, the silicone tube was washed with sonication for 0.5 h in ethanol and deionized water. The silicone tube surface was attached to carboxyl groups by a carboxyl silane coupling agent, and then, the liposome solution was poured into the tube and stored 12 h at room temperature. Then, clean the tube with deionized water.

2.5. Fluid-structure interaction simulation

Navier-Stokes equations,

$$\frac{\partial \rho_l}{\partial t} + \nabla \cdot (\rho_l \boldsymbol{u}) = 0 \tag{1}$$

$$\frac{\partial (\rho_l u)}{\partial t} + \nabla \cdot (\rho_l u \boldsymbol{u}) = \nabla \cdot (\mu \nabla u) - \frac{\partial p}{\partial x} + F_x \tag{2}$$

$$\frac{\partial (\rho_l \upsilon)}{\partial t} + \nabla \cdot (\rho_l \upsilon \boldsymbol{u}) = \nabla \cdot (\mu \nabla \upsilon) - \frac{\partial p}{\partial y} + F_y \tag{3}$$

$$\frac{\partial (\rho_l \omega)}{\partial t} + \nabla \cdot (\rho_l \omega \boldsymbol{u}) = \nabla \cdot (\mu \nabla \omega) - \frac{\partial p}{\partial z} + F_z \tag{4}$$

where ρ_l, p, and μ represent the fluid density, the pressure and the viscosity. u, v, w and F_x, F_y, F_z represent velocity's and body force's components in three directions respectively. Eq. (1) is the mass conservation equation, Eq. (2) ~ Eq. (4) are the momentum conservation equations.

The equilibrium equations for solid mechanics are given by the following equation.

$$\rho_s \frac{\partial^2 \boldsymbol{d}}{\partial t^2} = \nabla \cdot \boldsymbol{\sigma} + \boldsymbol{F}_b \tag{5}$$

where ρ_s is the material density, $\mathbf{d}$ is the vector of structure displacement, $\boldsymbol{\sigma}$ is Second Piola-Kirchhoff stress, $\mathbf{F}_b$ is the volume force vector.

Navier-Stokes equation provides a solution for the velocity field. The pressure and viscous forces in the fluid provide a load on the boundary of the solid.

$$\mathbf{f} = \mathbf{n} \cdot \left\{ -p\mathbf{I} + \left(\mu \left(\nabla \mathbf{u} + (\nabla \mathbf{u})^T \right) - \frac{2}{3} \mu (\nabla \cdot \mathbf{u}) \mathbf{I} \right) \right\} \tag{6}$$

where p denotes pressure, μ is the dynamic viscosity for the fluid, $\mathbf{n}$ is the outward normal to the boundary, and $\mathbf{I}$ is the identity matrix.

The simulation was conducted by a computational fluid dynamics (CFD) software COMSOL, and the simulated process was as follows. First, a 3D geometry of hydrogel in phosphate buffer saline (PBS) solution was created, and then the geometry was automatically divided into unstructured meshes. Next, a laminar flow model combined with solid mechanics model was added to the CFD solver. Afterward, we defined the materials in our cases. The density of PBS solution is 1070 kg/m^3 and the viscosity is 0.7 mPa s. Moreover, Young's modulus of hydrogel was set to 112.6 kPa and the Poisson's ratio of hydrogel was set to 0.236. Further, some necessary boundary conditions were set up. In the laminar flow model, the velocity inlet of PBS solution (110 mL/min), pressure outlet as well as non-slip wall condition were determined. Besides, the bottom of the hydrogel was set as fixed in the solid mechanics model. Finally, we calculated the steady-state fluid-structure interaction

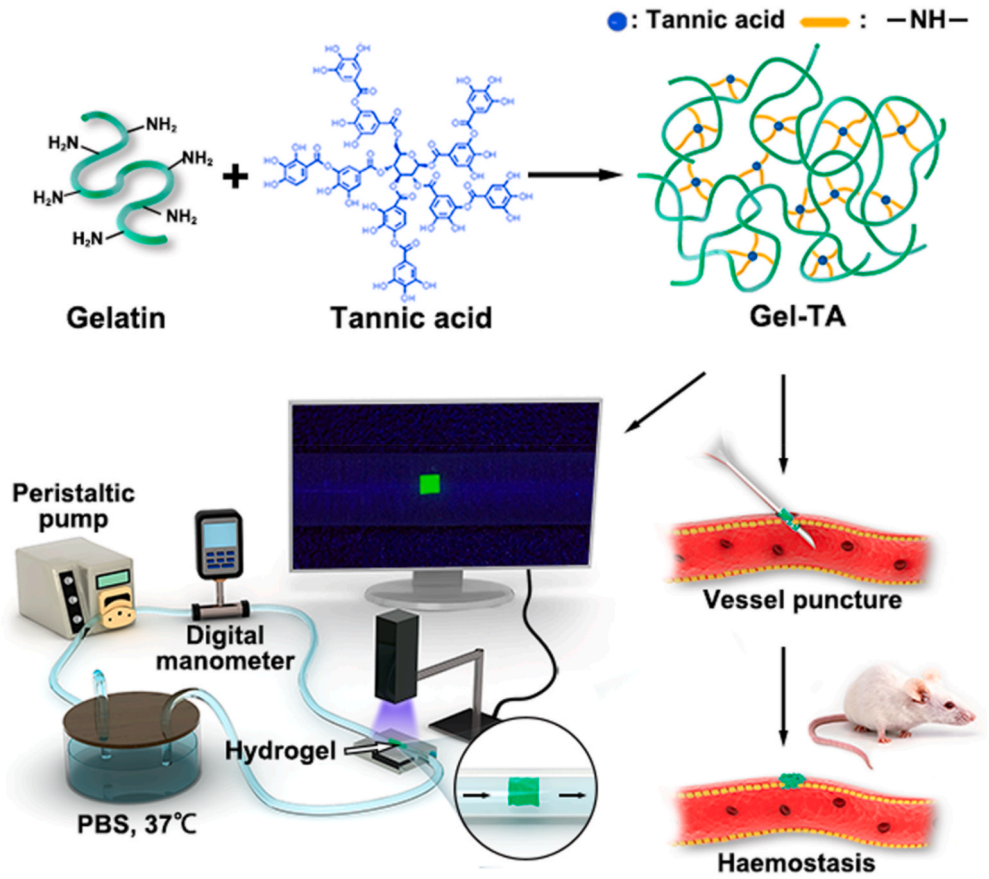

Scheme 1. Schematic illustration of the formation of adhesive hydrogel for vessel puncture haemostasis and illustration of the microfluidic setup for the *in vitro* evaluation of the adhesion of hydrogels on the simulated vessel.

simulation and analyzed the effect of different height/length ratios.

2.6. Preparation of haemostatic needles

Dissolve 50 mg of gelatin in 0.95 g of deionized water to obtain Gelatin solution (5 wt%). Then, add 100 mg of TA (10 wt%) to this solution and stir it at room temperature until it was homogeneous. Store the solution 48 h at room temperature before coating the needles. Then prepare the haemostatic needles as we described previously [17]. Amounts of Gel-TA solution was according to the gauge values of different commercial syringe needles: 18 G with 20 μL, 22 G with 4.5 μL, 25 G with 3 μL and 30 G 2 μL. Likewise, the FITC-Gel-TA-coated needles were obtained using a similar coating process.

2.7. Characterizations

NMR spectra were obtained using a Bruker AV400 NMR spectrometer. Atomic force microscopy (AFM, Shimadzu SPM-9700) and optical microscopy (Dino-lite microscope) measurements were also performed. Use an electronic digital caliper to obtain the length and thickness of coating. Conduct rheological measurements on an MCR-302 rheometer (Anton Paar). The Scanning electron microscopy (SEM) measurements, confocal luminescence images, storage modulus (G′) and loss modulus (G′) was determined as described previously [17].

2.8. Cytotoxicity evaluation of the Gel-TA

Quantitative CCK-8 cytotoxicity was used to evaluate the cytotoxicity of the hydrogels as we described previously [17].

2.9. Tissue puncture

The haemostatic effect of the Gel-TA-coated needle was evaluated by using the external jugular vein, inferior vena cava, and abdominal aorta of male Sprague-Dawley rats (250–300 g) and ear vein and femoral artery of female New Zealand white rabbits (2.5–3.0 kg). We conduct animal experiments under ethics protocol IACUC Number:2537 approved by the Institutional Animal Care and Use Committee, the Medical Ethics Committee of Tongji Medical College, Huazhong University of Science and Technology, Wuhan, China. Pentobarbital sodium was used to anesthetize animals by intraperitoneal injection (30–50 mg kg^{-1}). After anesthetization, we carefully dissected the rats and exposed the right external jugular vein, inferior vena cava, or abdominal aorta. Rabbits were carefully dissected and then exposed the femoral artery. The exposed blood vessel was punctured with a bare or haemostatic needle (22 G for the external jugular vein and inferior vena cava, and 30 G for the abdominal aorta and femoral artery), and withdrawn the needles after 15 s. The amount of blood loss was evaluated as we described previously [17]. The abdominal aortas of the mice punctured with Gel-TA-coated needles were collected either immediately after puncture or two weeks after the puncture for H-E staining. For rabbit ear vein haemostasis, puncture the rabbit ear vein with a Gel-TA-coated needle or bare needle (25 G). The amount of bleeding was calculated and measured as described above. Blood samples were collected from these rabbits at a given time and used for prothrombin time (PT) and partially activated thromboplastin time (aPTT) tests, blood cell count, creatinine (Cr), blood urea nitrogen (Bun) examination, or alanine transaminase (ALT), and aspartate aminotransferase (AST) examination.

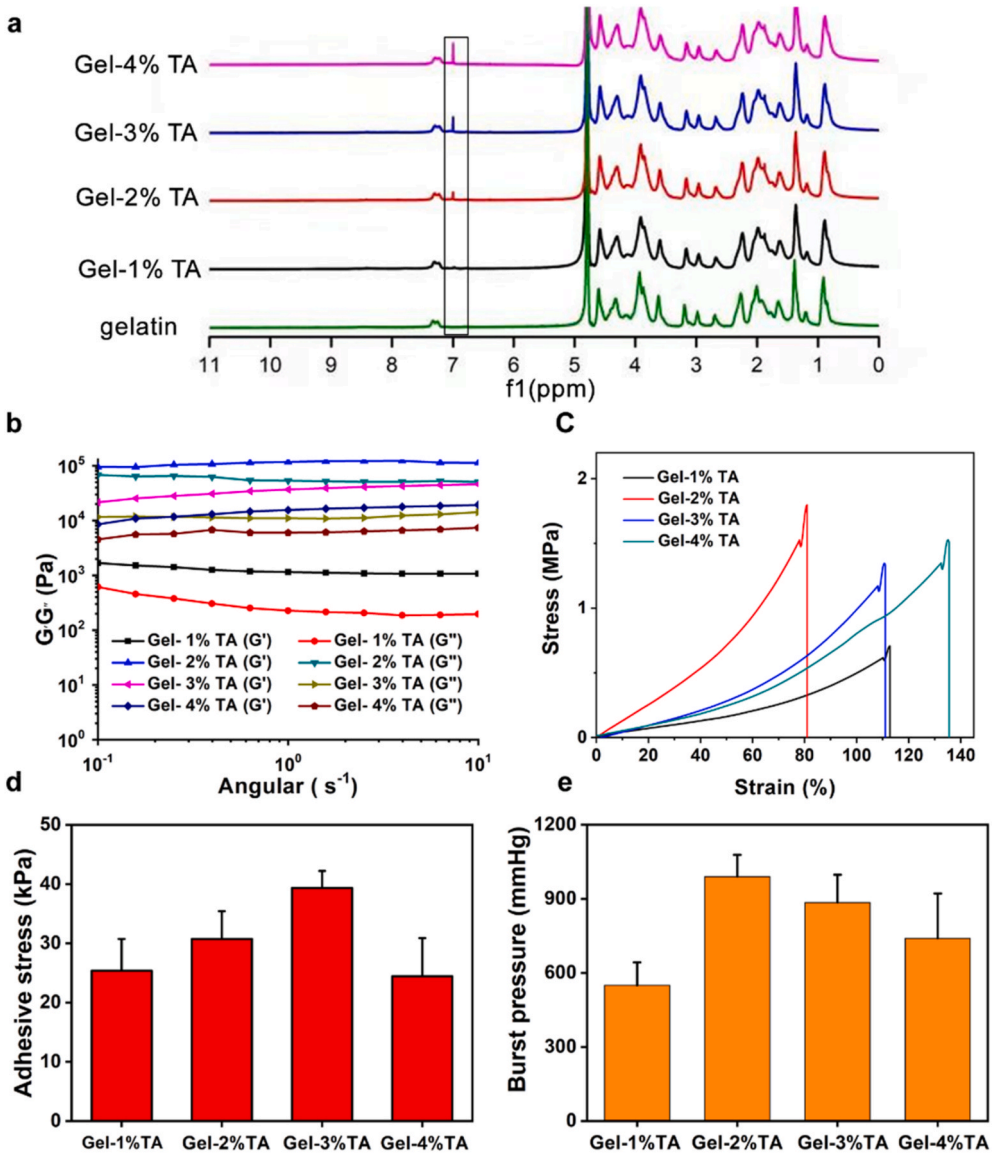

Fig. 1. Adhesion and mechanical properties of Gel-TA with different TA mass contents. a ^{1}H NMR spectra obtained in D_2O. b Rheological analysis of hydrogel films after swelling in the serum. c Strain–stress curves. d Adhesive strength to porcine skin and e burst pressures of Gel-1% TA, Gel-2% TA, Gel-3% TA, and Gel-4% TA hydrogels.

2.10. Statistical analysis

All data were expressed as mean ± SD. Statistical analyses were performed using SPSS 21.0. Significant differences were analyzed using Student's *t*-test. Statistical significance was defined as $p < 0.05$.

3. Results and discussion

3.1. Synthesis and characterization of Gel-TA

Gel-TA precursor solution was prepared to coat syringe needle surfaces and then dried with a lab-made rotating system to prepare haemostatic needles, which can swell during the puncture process and undergo a solid-to-hydrogel phase transition *in situ* to physically seal the puncture wounds and achieve haemostasis. By manipulating and controlling the microfluidic platform and miniaturized devices with vessel-sized channels, a microfluidic system was used to optimize the adhesion of Gel-TA. The process for preparing the haemostatic hydrogel was briefly illustrated in Scheme 1. First, a Gel-TA precursor solution was prepared *via* a facile Michael addition reaction of gelatin and TA between phenol and amine groups under oxidizing conditions at room temperature for 48 h. The relationship between the adhesive and mechanical properties of the material and the blood pressure can be effectively evaluated in the microfluidic channels [31–33]. The hydrogel used for the haemostatic needle coating needs to have better adhesive and mechanical properties than the stress levels microfluidic simulations show to reach *in situ* haemostasis during the puncture of different vessels.

Generally, to achieve haemostasis in the artery, the hydrogel should tightly and integrally adhere to the wounds under high blood pressure [21,34]. The mechanical and adhesive strength can be carefully adjusted by varying the mass ratio between the gelatin and TA in the hydrogel. Four groups of the samples with TA mass contents of 1%, 2%, 3%, and 4% (hereafter denoted by Gel-1% TA, Gel-2% TA, Gel-3% TA, Gel-4% TA) were thus prepared. The successful synthesis of the hydrogels was confirmed by ^{1}H NMR spectra, with the absorption peak increasing at ~6.8 ppm of phenol –OH groups of TA (Fig. 1a) [35]. The rheological analysis was employed to investigate the mechanical strength of the Gel-TA. As shown in Fig. 1b, the Gel-2% TA showed the best mechanical properties among the samples, as its storage modulus (G′) of 95.2 kPa

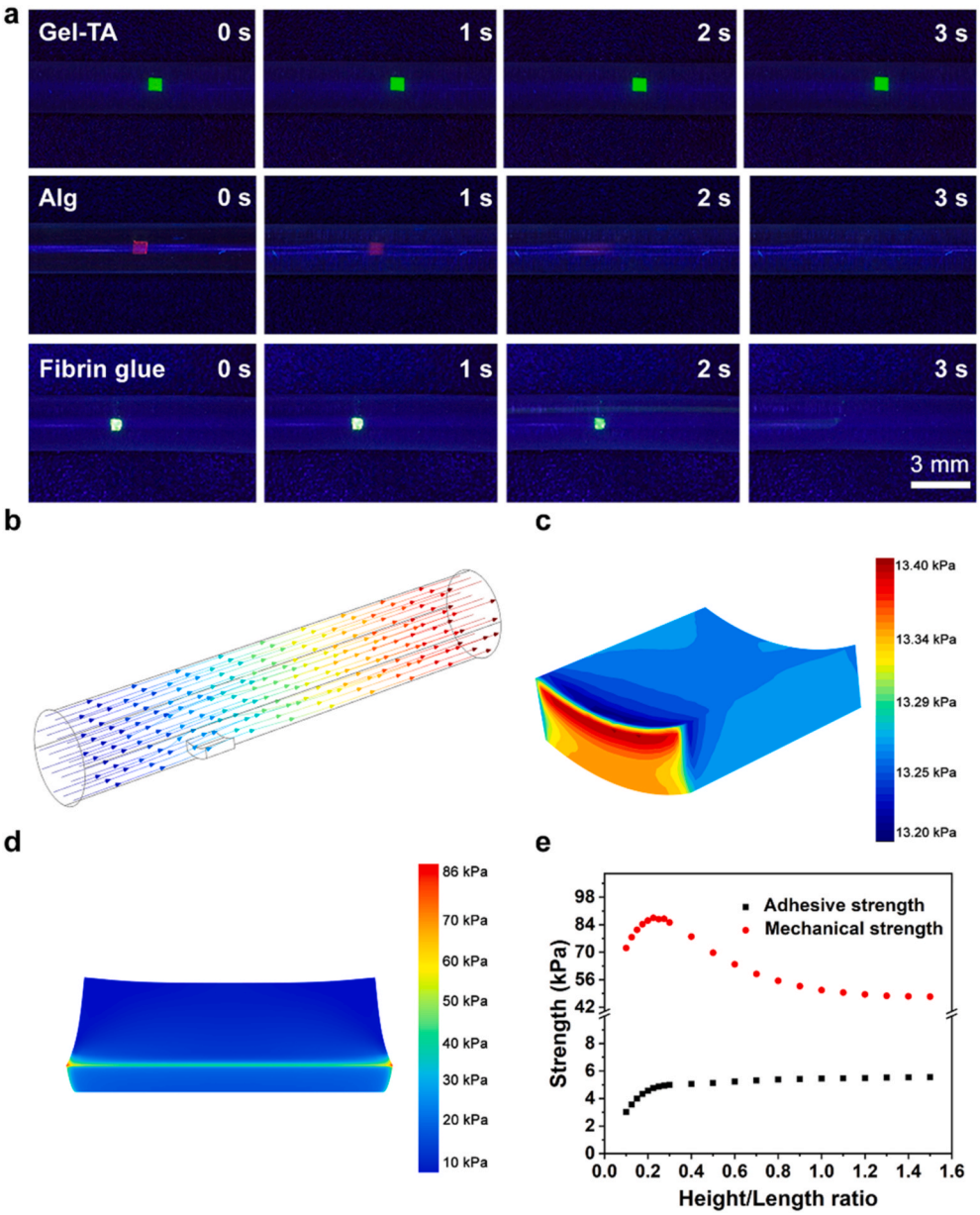

Fig. 2. Microfluidic system evaluation for the haemostatic coating. a Morphology of the FITC-Gel-TA, RhB-Alg, and sodium fluorescein fibrin glue in the simulated vessel under a pressure of 100 mmHg. b Schematic illustration of the CFD simulation of the hydrogel force distribution in PBS solution at 37 °C. c CFD simulations of the adhesive and d mechanical strength of the hydrogel in PBS solution at 37 °C. e Variation in the adhesive and mechanical strength with the ratio of the length to the height of the hydrogel.

was larger than its loss modulus (G″, 67.7 kPa). Similarly, its mechanical properties were confirmed by the strain-stress test, which showed that the Gel-2% TA had the highest strength value of 1.8 MPa (Fig. 1c). As the hydrogel must immediately adhere to the puncture site to stop the bleeding, the adhesive strength of the hydrogel is an important factor for vessel haemostasis. Therefore, we used the lap shear strength test to assess the adhesive strength of the above samples. In detail, the tests were performed after the samples (adhesive area: 2 mm × 2 mm) were swollen in a PBS solution and then adhered to porcine skin. The results showed that the adhesive strengths of Gel-TA with different TA mass content were 25.3 kPa, 30.7 kPa, 39.3 kPa, and 24.4 kPa (Fig. 1d). The burst pressure test is the main efficacy test relevant to evaluate the capacity of the hydrogels to withstand blood pressure, while rapidly adhering to tissues to seal the rupture [21]. Based on previous reports, we prepared a series of 22 G haemostatic needles with hydrogel coatings of different TA mass contents [12,17]. After puncture with the haemostatic needles, the hydrogel was formed *in situ* on the porcine skin in a chamber linked to a syringe pump, which was filled with PBS solution (Fig. S1). All of the hydrogels showed a higher burst pressure than normal blood pressure (100 mmHg) (Fig. 1e). Furthermore, the Gel-2% TA hydrogel showed the highest burst pressure (990 mmHg).

Furthermore, the maximum flow velocity of Gel-1% TA, Gel-2% TA, Gel-3% TA, and Gel-4% TA hydrogels sustained was evaluated using microfluidic devices that simulate the vessels in vitro. Silicone tube is widely used in the production of surgical line catheters, vascular access catheters, blood bags etc. Liposome-decorated silicone tube can suppress platelet adhesion on the silicon catheter surface with a simulative endothelial cell layer of blood vessels [36]. Then, we adopted a liposome-decorated silicone tube (inner diameter 2 mm) to simulate the blood vessels. X-ray photoelectron spectroscopy (XPS) measurements were used to confirm the successful decoration of the liposome with the appearance of N and P signals associated with the liposome (Figs. S2a–c and Table S1). The water contact angle of the liposome-decorated silicone tube was 77.1 ± 1.3°, which was similar to that of the blood vessels (Fig. S2d) [36]. To systematically optimize Gel-TA, the fluorescein-labeled Gel-TA with different TA amounts were prepared with a volume of ~1 mm × 1 mm × 0.5 mm, and then adhered to the inner silicon tube wall. The Gel-2% TA displayed the highest flow

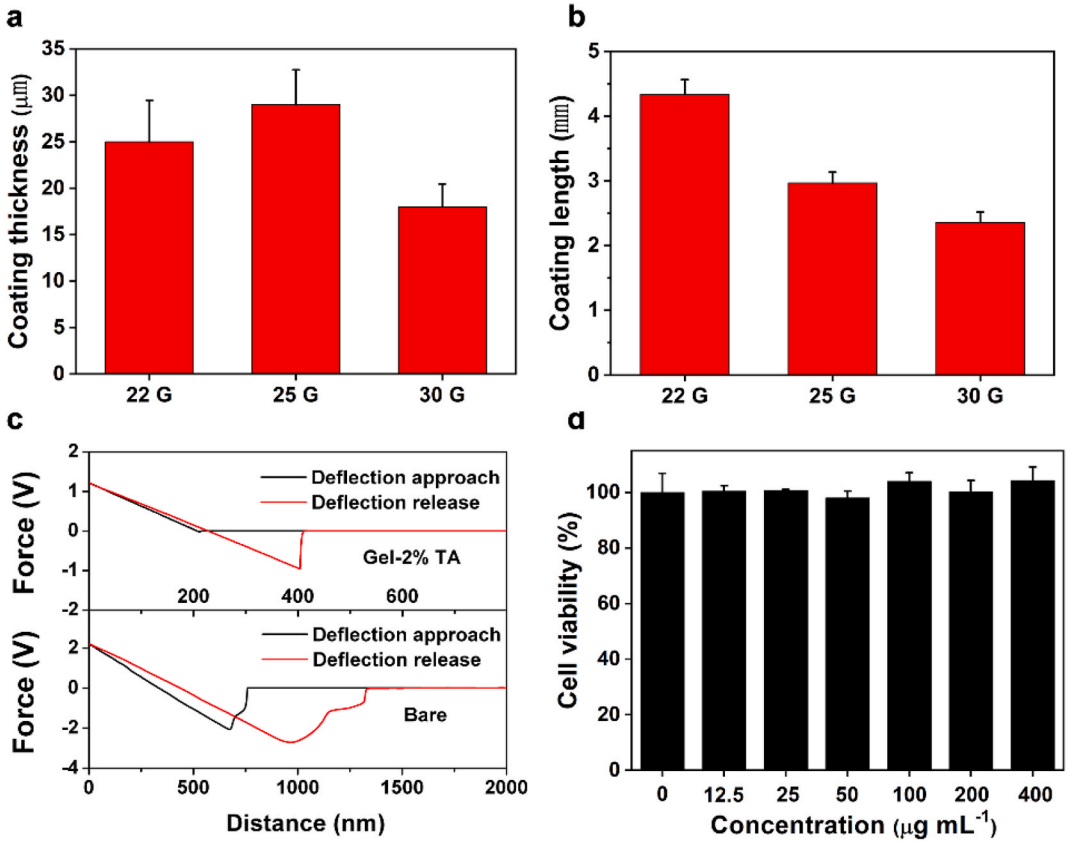

Fig. 3. Characterization of the haemostatic needles. a Thickness and b length of the coating on (left to right) 22 G, 25 G, and 30 G haemostatic needles. c The friction of needles. d Cytocompatibility evaluation of the Gel-TA.

velocity (260 ± 12.65 mL/min) (Fig. S3), which was consistent with the burst pressure of the hydrogels. Therefore, the Gel-2% TA was chosen to evaluate the relationship between the adhesive strength and mechanical strength and different vessels using microfluidic devices. We found that fluorescein-labeled Gel-TA adhered tightly to the inner surface without any morphological changes under normal artery pressure (100 mmHg) (Fig. 2a). However, alginate-Ca (Alg) hydrogel and fibrin glue, a kind of commercially available surgical glues, used for low-pressure vessel haemostasis, were quickly washed away in this condition (Fig. 2a). Compared to Gel-TA (30.7 kPa) hydrogel, the adhesion of Alg (2.3 kPa) hydrogel and fibrin glue (8.6 kPa) were much lower (Fig. S4). To calculate the adhesive and mechanical strength of the hydrogel in PBS solution, the finite element method was utilized to simulate the fluid-structure interaction process in a three-dimensional model. Fluid-Structure Interaction involves several phenomena where fluid and a solid structure interact with each other. The flow process is described by Navier-Stokes equation, and the adhesive strength as well as the mechanical strain of the hydrogel is calculated by the equilibrium equation of solid mechanics, where the pressure and viscous forces of PBS solution provide a load on the boundary of the hydrogel. In our study, the Gel-2% TA hydrogel was adopted for simulation, Young's modulus and Poisson's ratio of which were set to112.6 kPa and 0.236, respectively. The velocity inlet of PBS solution was set to 110 mL/min, and then pressure outlet, as well as non-slip wall condition, were determined. Besides, the bottom of the hydrogel was set as fixed in the solid mechanics model. In theory, the underwater adhesion of the hydrogel was 4.9 kPa, and the mechanical strength was 86.0 kPa under normal blood pressure (100 mmHg) (Fig. 2b–d). We found that the adhesive and mechanical strength both varied with the increasing length-to-height ratio of the hydrogel (Fig. 2e). Notably, this is only suitable for the hydrogel to adhere to the inner wall of blood vessels. Although fibrin glue can theoretically satisfy the above demand of adhesion strength under normal blood pressure (100 mmHg), it does not have the durable underwater adhesion as Gel-TA with catechol structure.

3.2. Characterization of the haemostatic needles

To further evaluate the *in vivo* haemostatic effect of the Gel-TA, Gel-TA-coated needles were prepared. Typically, a precursor solution for the Gel-2% TA was prepared, then drop onto the needles surface 2 mm away from the tip, then finally dried with a lab-made rotating system. SEM and Energy-dispersive X-ray spectrometry (EDS) were used to confirmed the successful uniform coating, with the existence of the C and N signals associated with gelatin and TA, and the uncoated site showed Fe, Cr, and Mn signals (Fig. S5). The length and thickness of the coating were tuned according to the requirements of different needles and in the present study, the existing coating length and thickness can meet the haemostatic requirements (Fig. 3a and b). Moreover, the haemostatic needles (22 G) exhibited a much lower friction force than the bare needles (Fig. 3c).

Furthermore, by coincubation with 3T3 fibroblasts, we conducted CCK-8 assay for cellular viability, which was above 95%, revealing the excellent biocompatibility of Gel-TA (Fig. 3d).

3.3. Haemostatic evaluation after vein puncture

To evaluate the haemostatic efficiency of Gel-TA *in vivo*, we first tested the haemostatic effect of a Gel-TA-coated needle on veins with different blood pressures by puncturing the external jugular vein and inferior vena cava of rats and the ear vein of rabbits. Specifically, we used a 22 G needle coated with Gel-TA to perform puncture of rat external jugular vein. After anatomizing the right external jugular veins, 22 G haemostatic needles were used to puncture the external jugular

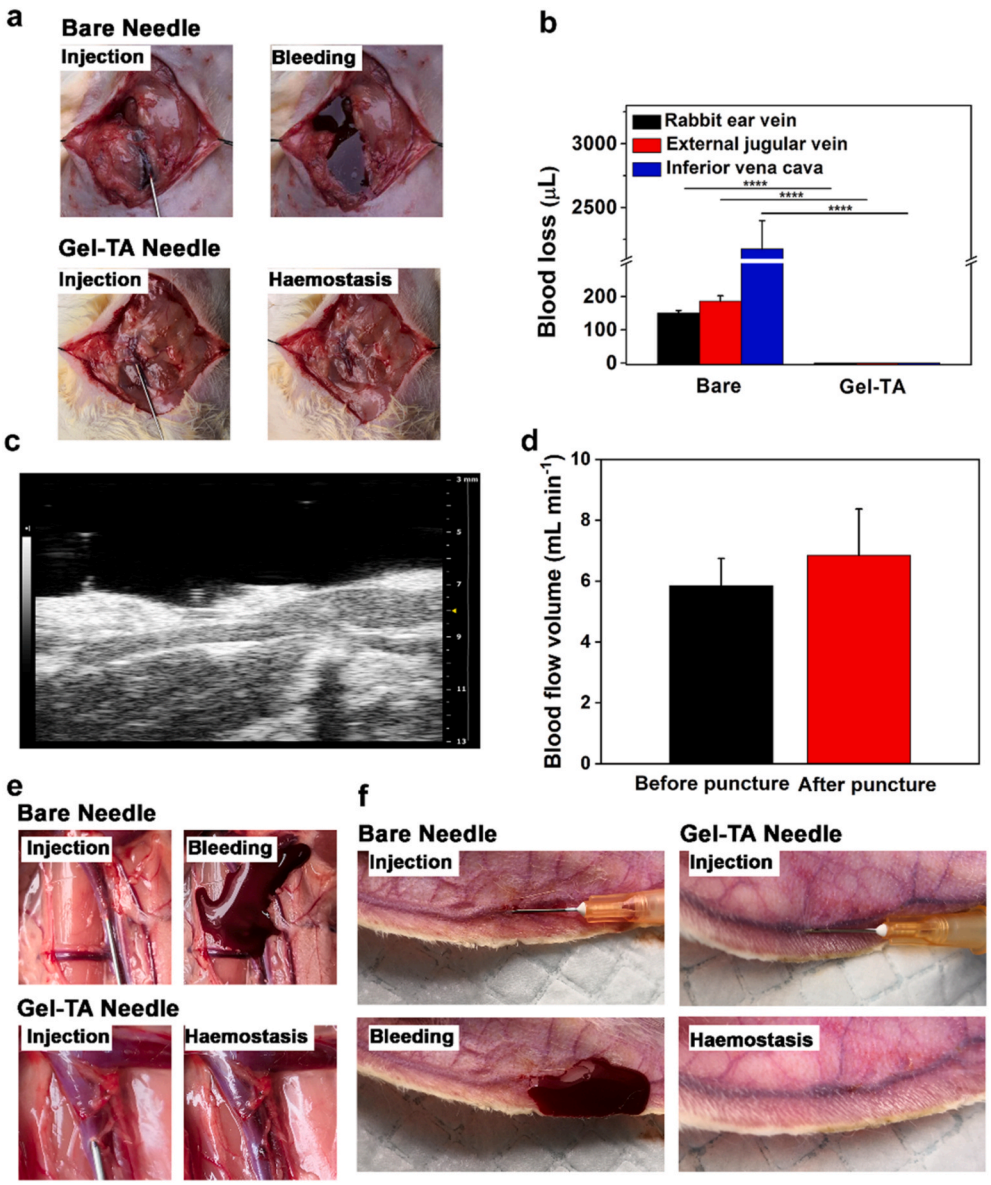

Fig. 4. Haemostatic properties of the Gel-TA-coated needles in venipuncture. a Images of rat external jugular vein puncture: the top is bare needle and the bottom is Gel-TA-coated needle. b Quantitative analysis of bleeding from rat external jugular vein (n = 4, ****p < 0.0001), rat inferior vena cava (n = 4, ****p < 0.0001) and rabbit ear vein (n = 4, ****p < 0.0001). c High-resolution ultrasound image of the external jugular vein after punctured by haemostatic needle. d Blood flow volume of external jugular vein before and after puncture with Gel-TA-coated 22 G needles (n = 6, p > 0.05). e Images of rat inferior vena cava puncture: top is bare needle and bottom is Gel-TA-coated needle. f Images of rabbit ear vein puncture: left is bare needle and right is Gel-TA-coated needle.

veins, with bare needles as controls. We observed no blood loss in the Gel-TA-coated 22 G needle group (Fig. 4a and b and Movie S1), whereas blood obviously flowed out from the external jugular vein punctured by the bare needle, with a mean bleeding amount of 185.9 ± 16.1 μL (Fig. 4a and b and **Movie S**2). Subsequently, small animal ultrasound was used to investigate the vascular lumen and blood flow volume before and after puncture using a haemostatic needle. Our results showed that the blood vessel was unobstructed without obvious stenosis or thrombosis, and the blood flow volume did not change after puncturing with a Gel-TA-coated needle (Fig. 4c and d).

To assess the haemostatic capacity of the haemostatic needle in vein with higher pressure, inferior vena cava in rats was punctured. As shown in Fig. 4b, e and Movie S3, the Gel-TA-coated needles (22G) showed complete haemostasis after puncture. Conversely, puncturing with bare needles led to obvious bleeding with a mean bleeding amount of 2.1 ± 0.2 mL (Fig. 4b, e and Movie S4). The rabbit ear vein, which is relatively superficial, belongs to percutaneous puncture, and can better simulate the operation of venipuncture in the clinic. When the rabbit ear vein was punctured, the bare needle (25G) again caused obvious bleeding, with a mean bleeding amount of 150.2 ± 7.5 μL (Fig. 4b, f), whereas no bleeding was observed in the Gel-TA-coated needle (Fig. 4b, f). In addition, we further confirmed that the Gel-TA coating would not detach from the needle before being pulled out from the blood vessel (Fig. S6). Moreover, after puncture, rabbit blood samples were collected to analyze PT and aPTT. No significant differences were found between the two groups, indicating that systemic coagulation function was not influenced by Gel-TA (Fig. 5a). Meanwhile, Cr, Bun, ALT, and AST were detected at 12 h after the puncture. We also tested blood cell counts at day 0, day 1, day 7, and day 14 after puncture to assess the biocompatibility of the Gel-TA coating. Our results showed that the Gel-TA-coated needle exhibited no significant effect on Cr, Bun, ALT, AST, or blood cell count, similar to the bare needle (Fig. 5b–g), suggesting the good biocompatibility of Gel-TA. In addition, during continuous observation for 14 days, no obvious inflammation occurred at the puncture site of the rabbit ear vein in either group. To evaluate the *in vivo* degradability of Gel-TA, we used haemostatic needle coated with Cy5-labeled Gel-TA to puncture mice external jugular vein. The results measured by the imaging system revealed that the fluorescent signal gradually decreased, and the Gel-TA was completely degraded on the tenth day (Fig. 6) [26,35].

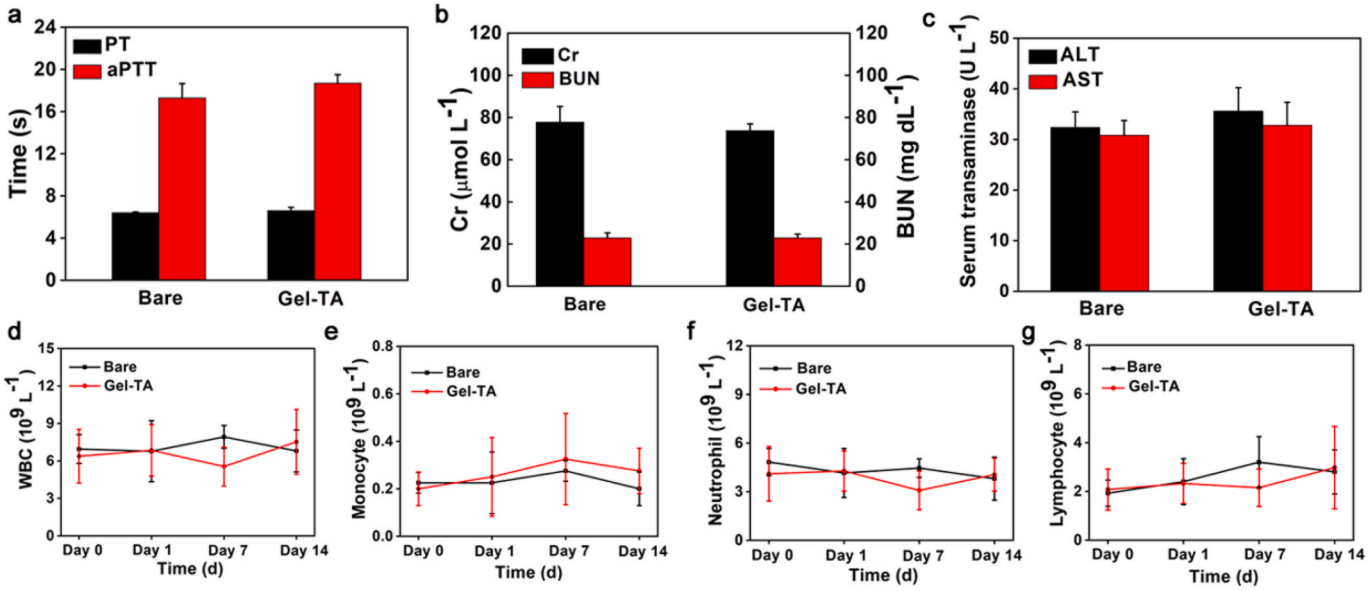

Fig. 5. Good biocompatibility of Gel-TA. a PT and aPTT tests (n = 4, p > 0.05). b,c Histogram showing Cr, Bun, ALT, and AST 12 h after puncture (n = 4, p > 0.05). d–g Plots showing blood cell count analysis for levels of white blood cells (WBCs), monocytes, neutrophils, and lymphocytes after puncture with the Gel-TA-coated and bare needles (n = 4, p > 0.05).

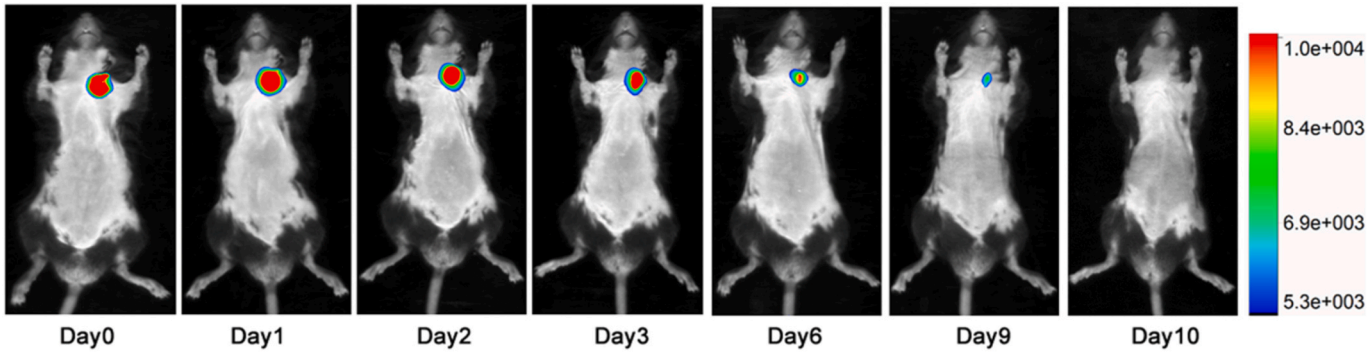

Fig. 6. *In vivo* imaging of Gel-TA haemostatic coating labeled by Cy5 (n = 3).

3.4. Haemostatic evaluation in arterial puncture

Compared with venipuncture, haemostasis in arterial puncture is more difficult because of the higher blood pressure. To examine the haemostatic effect of the Gel-TA-coated needle in arterial puncture, the abdominal aorta of rats was punctured using either a Gel-TA-coated 30 G needle or a bare needle as a control. The haemostatic effect of Gel-TA-coated needles was compared with the bare needles. Specifically, the haemostatic needles completely prevented bleeding, while bare needle induced blood loss of 1.7 ± 0.2 mL (Fig. 7a and b and Movie S5, 6). To validate that the hydrogel could physically seal the wound, abdominal aortas punctured by haemostatic needles were collected and analyzed using H-E staining. The detached Gel-TA was observed in the vessel inner wall and did not block the lumen of the abdominal aorta (Fig. 7c). In addition, to moitor the healing of the abdominal aorta punctured by Gel-TA-coated needle, another abdominal aorta was collected for H-E staining two weeks after the puncture. The results showed that no residual hydrogel was found, and the wound was almost completely healed (Fig. S7). In clinical practice, femoral arterial puncture is often used for blood gas analysis [37]. We punctured rabbit femoral arteries to confirm the haemostatic capacity of the Gel-TA-coated needles. Clearly, the bare needle (30G) caused significant bleeding with a bleeding amount of 604.2 ± 17.9 μL (Fig. 7b, d and Movie S7). In comparison, haemostatic needles caused no bleeding (Fig. 7b, d and Movie S8). Taken together, the results demonstrate that for both vein and arterial puncture of different animal models, Gel-TA-coated needles exhibit synchronous haemostasis through an *in situ* solid-to-gel phase transition. The previously reported haemostatic needles attained haemostasis in vein puncture because of the low vein pressure. However, owing to the limited underwater adhesion and weak bonding mechanics of those hydrogels, they failed to stop bleeding in the arterial puncture. In contrast, the current Gel-TA with both high adhesive and mechanical strength can effectively achieve haemostasis in arterial puncture.

4. Conclusions

In summary, we have developed a novel microfluidic platform to assess the relationship between the adhesion of haemostatic needle coatings and blood vessel pressure. Additionally, the adhesive strength of Gel-TA could be controlled by varying the components of gelatin and TA. To achieve haemostasis in arterial puncture, the underwater adhesion of the hydrogel should be higher than 4.9 kPa, and the mechanical strength should be higher than 86.0 kPa. In different animal models, the Gel-TA-coated needles can completely prevent bleeding after both vein and arterial puncture. This study provides valid evidence for preparing haemostatic needles for different vessels.

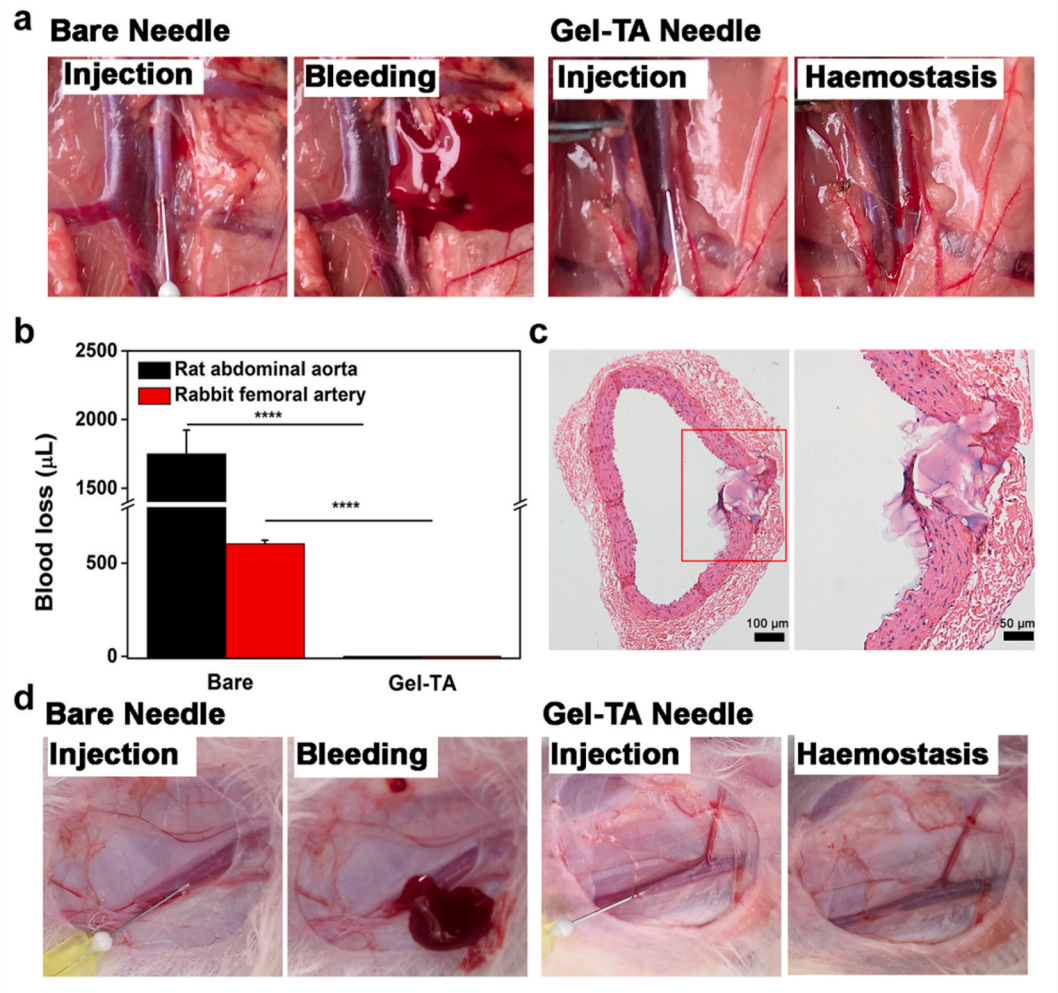

Fig. 7. Evaluation of the haemostatic capability of the haemostatic needles in arterial puncture. a Images of rat abdominal aorta puncture: bare needle (left) and Gel-TA-coated needle (right). b Quantitative analysis of bleeding from rat abdominal aorta puncture ($n = 4$, ****$p < 0.0001$) and rabbit femoral arterial puncture ($n = 4$, ****$p < 0.0001$). c H-E staining of a rat abdominal aorta punctured by Gel-TA-coated needle (30 G). d Images of rabbit femoral artery puncture: left is bare needle and right is Gel-TA-coated needle.

Declaration of interests

The authors declare that they have no known competing financial interests or personal relationships that could have appeared to influence the work reported in this paper.

CRediT authorship contribution statement

Xingjie Yin: Conceptualization, Methodology, Investigation, Writing original draft. **Jingli Ren:** Conceptualization, Methodology, Investigation, Writing original draft. **Wei Lan:** Investigation, Formal analysis. **Yu Chen:** Investigation, Validation. **Mengping Ouyang:** Methodology. **Hua Su:** Validation, Formal analysis. **Lianbin Zhang:** Project administration, Funding acquisition. **Jintao Zhu:** Writing – review & editing, Supervision. **Chun Zhang:** Writing – review & editing, Project administration, Funding acquisition.

Declaration of competing interest

The authors declare no competing interests.

Acknowledgements

This work was supported by the National Natural Science Foundation of China (81961138007, 81974096, 81770711, and 52022032).

Appendix A. Supplementary data

Supplementary data to this article can be found online at https://doi.org/10.1016/j.bioactmat.2021.10.009.

References

[1] Z.M. Younossi, R. Loomba, Q.M. Anstee, M.E. Rinella, E. Bugianesi, G. Marchesini, B.A. Neuschwander-Tetri, L. Serfaty, F. Negro, S.H. Caldwell, V. Ratziu, K.E. Corey, S.L. Friedman, M.F. Abdelmalek, S.A. Harrison, A.J. Sanyal, J.E. Lavine, P. Mathurin, M.R. Charlton, Z.D. Goodman, N.P. Chalasani, K.V. Kowdley, J. George, K. Lindor, Diagnostic modalities for nonalcoholic fatty liver disease, nonalcoholic steatohepatitis, and associated fibrosis, Hepatology 68 (1) (2018) 349–360.

[2] S.J. Barbour, R. Coppo, H. Zhang, Z.H. Liu, Y. Suzuki, K. Matsuzaki, R. Katafuchi, L. Er, G. Espino-Hernandez, S.J. Kim, H.N. Reich, J. Feehally, D.C. Cattran, Evaluating a New international risk-prediction tool in IgA nephropathy, JAMA Intern. Med. 179 (7) (2019) 942–952.

[3] Y. Chen, Z. Ke, J. Xiao, M. Lin, X. Huang, C. Yan, S. Ye, X. Tan, Subcutaneous injection of nitroglycerin at the radial artery puncture site reduces the risk of early radial artery occlusion after transradial coronary catheterization: a randomized, placebo-controlled clinical trial, Circ Cardiovasc Interv 11 (7) (2018), e006571.

[4] S. Schulz-Schüpke, S. Helde, S. Gewalt, T. Ibrahim, M. Linhardt, K. Haas, K. Hoppe, C. Böttiger, P. Groha, C. Bradaric, R. Schmidt, L. Bott-Flügel, I. Ott, J. Goedel, R. A. Byrne, S. Schneider, C. Burgdorf, T. Morath, S. Kufner, M. Joner, S. Cassese, P. Hoppmann, C. Hengstenberg, J. Pache, M. Fusaro, S. Massberg, J. Mehilli, H. Schunkert, K.L. Laugwitz, A. Kastrati, Comparison of vascular closure devices vs

manual compression after femoral artery puncture: the ISAR-CLOSURE randomized clinical trial, Jama 312 (19) (2014) 1981–1987.
[5] D.G. Moledina, R.L. Luciano, L. Kukova, L. Chan, A. Saha, G. Nadkarni, S. Alfano, F. P. Wilson, M.A. Perazella, C.R. Parikh, Kidney biopsy-related complications in hospitalized patients with acute kidney disease, Clin. J. Am. Soc. Nephrol. 13 (11) (2018) 1633–1640.
[6] A. Srinivasan, A.K. Guzman, E.B. Rand, J. Rychik, D.J. Goldberg, P.A. Russo, A. M. Cahill, Percutaneous liver biopsy in Fontan patients, Pediatr. Radiol. 49 (3) (2019) 342–350.
[7] M.A.C. Campos, C.M.R. Alves, M.H. Tsunemi, M.A.S. Peterlini, A.F.M. Avelar, Randomized clinical study on radial artery compression time after elective coronary angiography, Rev Lat Am Enfermagem 26 (2018), e3084.
[8] L.J. Wentworth, E.L. Bechtum, J.G. Hoffman, R.R. Kramer, D.C. Bartel, J.P. Slusser, R.T. Tilbury, Decreased bed rest post-percutaneous coronary intervention with a 7-French arterial sheath and its effects on vascular complications, J. Clin. Nurs. 27 (1–2) (2018) e109–e115.
[9] E. Caturelli, M.M. Squillante, A. Andriulli, D.A. Siena, C. Cellerino, F. De Luca, M. A. Marzano, M. Pompili, G.L. Rapaccini, Fine-needle liver biopsy in patients with severely impaired coagulation, Liver 13 (5) (1993) 270–273.
[10] J. Bandari, T.W. Fuller, U.i.U.R.M. Turner capital, L.A. D'Agostino, Renal biopsy for medical renal disease: indications and contraindications, Can. J. Urol. 23 (1) (2016) 8121–8126.
[11] M.I. Rodriguez, J.T. Jensen, K. Gregory, M. Bullard, P. Longo, J. Heidel, A. Edelman, A novel tamponade agent for management of post partum hemorrhage: adaptation of the Xstat mini-sponge applicator for obstetric use, BMC Pregnancy Childbirth 17 (1) (2017) 187.
[12] M. Shin, S.G. Park, B.C. Oh, K. Kim, S. Jo, M.S. Lee, S.S. Oh, S.H. Hong, E.C. Shin, K.S. Kim, S.W. Kang, H. Lee, Complete prevention of blood loss with self-sealing haemostatic needles, Nat. Mater. 16 (1) (2017) 147–152.
[13] Z. Qiao, X. Lv, S. He, S. Bai, X. Liu, L. Hou, J. He, D. Tong, R. Ruan, J. Zhang, J. Ding, H. Yang, Bioactive materials 6 (9) (2021) 2829–2840.
[14] C. Yan, T. Yang, S. Zhu, H. Wu, Synthesis and properties of poly(DEX-GMA/AAc) microgel particle as a hemostatic agent, Mater. Chem. 5 (20) (2017) 3697–3705.
[15] L. Gao, S. Ma, J. Luo, G. Bao, Y. Wu, F. Zhou, Y. Liang, Synthesizing functional biomacromolecular wet adhesives with typical gel–sol transition and shear-thinning features, ACS Biomater. Sci. Eng. 5 (9) (2019) 4293–4301.
[16] R. Xu, S. Ma, Y. Wu, H. Lee, F. Zhou, W. Liu, Adaptive control in lubrication, adhesion, and hemostasis by Chitosan-Catechol-pNIPAM, Biomater. Sci. 7 (9) (2019) 3599–3608.
[17] J. Ren, X. Yin, Y. Chen, Y. Chen, H. Su, K. Wang, L. Zhang, J. Zhu, C. Zhang, Alginate hydrogel-coated syringe needles for rapid haemostasis of vessel and viscera puncture, Biomaterials 249 (2020) 120019.
[18] T.M. McKeever, G. Hearson, G. Housley, C. Reynolds, W. Kinnear, T.W. Harrison, A.M. Kelly, D.E. Shaw, Using venous blood gas analysis in the assessment of COPD exacerbations: a prospective cohort study, Thorax 71 (3) (2016) 210–215.
[19] P.J. Mason, B. Shah, J.E. Tamis-Holland, J.A. Bittl, M.G. Cohen, J. Safirstein, D. E. Drachman, J.A. Valle, D. Rhodes, I.C. Gilchrist, An update on radial artery access and best practices for transradial coronary angiography and intervention in acute coronary syndrome: a scientific statement from the American heart association, circulation, Circ Cardiovasc Interv 11 (9) (2018), e000035.
[20] Y. Sandoval, M.N. Burke, A.S. Lobo, D.L. Lips, A.H. Seto, I. Chavez, P. Sorajja, M. S. Abu-Fadel, Y. Wang, A. Poulouse, M. Gössl, M. Mooney, J. Traverse, D. Tierney, E.S. Brilakis, Contemporary arterial access in the cardiac catheterization laboratory, JACC Cardiovasc. Interv. 10 (22) (2017) 2233–2241.
[21] Y. Hong, F. Zhou, Y. Hua, X. Zhang, C. Ni, D. Pan, Y. Zhang, D. Jiang, L. Yang, Q. Lin, Y. Zou, D. Yu, D.E. Arnot, X. Zou, L. Zhu, S. Zhang, H. Ouyang, A strongly adhesive hemostatic hydrogel for the repair of arterial and heart bleeds, Nat. Commun. 10 (1) (2019) 2060.
[22] E. Delamarche, D. Juncker, H. Schmid, Microfluidics for processing surfaces and miniaturizing biological assays, Adv. Mater. 17 (24) (2005) 2911–2933.
[23] Y. Yang, X. Zhao, J. Yu, X. Chen, R. Wang, M. Zhang, Q. Zhang, Y. Zhang, S. Wang, Y. Cheng, Bioactive materials 6 (11) (2021) 3962–3975.
[24] H. Lee, W.I. Kim, W. Youn, T. Park, S. Lee, T.S. Kim, J.F. Mano, I.S. Choi, Iron gall ink revisited: in situ oxidation of Fe(II)-Tannin complex for fluidic-interface engineering, Adv. Mater. 30 (49) (2018), e1805091.
[25] L. Zhou, L. Fan, X. Yi, Z. Zhou, C. Liu, R. Fu, C. Dai, Z. Wang, X. Chen, P. Yu, D. Chen, G. Tan, Q. Wang, C. Ning, Soft conducting polymer hydrogels cross-linked and doped by tannic acid for spinal cord injury repair, ACS Nano 12 (11) (2018) 10957–10967.
[26] S. Bahmanzadeh, T. Ruzgas, J. Sotres, Proteolytic degradation of gelatin-tannic acid multilayers, J. Colloid Interface Sci. 526 (2018) 244–252.
[27] Y. Wang, L. Li, Y. Ma, Y. Tang, Y. Zhao, Z. Li, W. Pu, B. Huang, X. Wen, X. Cao, J. Chen, W. Chen, Y. Zhou, J. Zhang, Multifunctional supramolecular hydrogel for prevention of epidural adhesion after laminectomy, ACS Nano 14 (7) (2020) 8202–8219.
[28] S. Ge, N. Ji, S. Cui, W. Xie, M. Li, Y. Li, L. Xiong, Q. Sun, Coordination of covalent cross-linked gelatin hydrogels via oxidized tannic acid and ferric ions with strong mechanical properties, J. Agric. Food Chem. 67 (41) (2019) 11489–11497.
[29] P. Podsiadlo, M. Michel, J. Lee, E. Verploegen, N. Wong Shi Kam, V. Ball, J. Lee, Y. Qi, A.J. Hart, P.T. Hammond, N.A. Kotov, Exponential growth of LBL films with incorporated inorganic sheets, Nano Lett. 8 (6) (2008) 1762–1770.
[30] J. Xie, C. Yang, Q. Liu, J. Li, R. Liang, C. Shen, Y. Zhang, K. Wang, L. Liu, K. Shezad, M. Sullivan, Y. Xu, G. Shen, J. Tao, J. Zhu, Z. Zhang, Encapsulation of hydrophilic and hydrophobic peptides into hollow mesoporous silica nanoparticles for enhancement of antitumor immune response, Small 13 (40) (2017) 1701741.
[31] Y. Chen, H.N. Chan, S.A. Michael, Y. Shen, Y. Chen, Q. Tian, L. Huang, H. Wu, A microfluidic circulatory system integrated with capillary-assisted pressure sensors, Lab Chip 17 (4) (2017) 653–662.
[32] X. Wang, D.T.T. Phan, D. Zhao, S.C. George, C.C.W. Hughes, A.P. Lee, An on-chip microfluidic pressure regulator that facilitates reproducible loading of cells and hydrogels into microphysiological system platforms, Lab Chip 16 (5) (2016) 868–876.
[33] K. Sato, K. Sato, Recent progress in the development of microfluidic vascular models, Anal. Sci. 34 (7) (2018) 755–764.
[34] X. Zhao, B. Guo, H. Wu, Y. Liang, P.X. Ma, Injectable antibacterial conductive nanocomposite cryogels with rapid shape recovery for noncompressible hemorrhage and wound healing, Nat. Commun. 9 (1) (2018) 2784.
[35] J. Guo, W. Sun, J.P. Kim, X. Lu, Q. Li, M. Lin, O. Mrowczynski, E.B. Rizk, J. Cheng, G. Qian, J. Yang, Development of tannin-inspired antimicrobial bioadhesives, Acta Biomater. 72 (2018) 35–44.
[36] O.D. Krishna, K. Kim, Y. Byun, Covalently grafted phospholipid monolayer on silicone catheter surface for reduction in platelet adhesion, Biomaterials 26 (34) (2005) 7115–7123.
[37] O. Spelten, F. Fiedler, R. Schier, W.A. Wetsch, J. Hinkelbein, Transcutaneous $PTCCO_2$ measurement in combination with arterial blood gas analysis provides superior accuracy and reliability in ICU patients, J. Clin. Monit. Comput. 31 (1) (2017) 153–158.